Novel Near-infrared Pump Wavelengths for Dysprosium Fiber Lasers

Md. Ziaul Amin, Matthew R. Majewski, Robert I. Woodward, Alexander Fuerbach, and Stuart D. Jackson

***Abstract*—We report two new near-infrared pump wavelengths at 0.8 μm and 0.9 μm for dysprosium (Dy^{3+})-doped mid-infrared fiber lasers, which are free from detrimental pump excited state absorption that has limited all previous Dy^{3+} fiber lasers using longer near-infrared pump wavelengths (i.e., 1.1 μm, 1.3 μm, and 1.7 μm). The maximum measured laser slope efficiencies were 18.5% and 23.7% with respect to launched pump power for 0.8 μm and 0.9 μm pump wavelengths, respectively. These new pump wavelengths provide higher fractional Stokes limits (which are 70% and 79% for 0.8 μm and 0.9 μm pumping wavelengths, respectively) than previous demonstrations. While our measured efficiencies are still below the Stokes limit, we have identified the causes to be background loss and multi-mode behaviour at the pump wavelengths; both easily solvable for future systems. A numerical model was used to confirm performance, paving the way to efficient future near-infrared-pumped, potentially diode-pumped Dy^{3+} fiber lasers emitting in the mid-infrared.**

***Index Terms*—Dysprosium, diode-pumped, fiber laser, near-infrared, mid-infrared.**

I. Introduction

THE development of cost-effective, compact, high-power and high-brightness mid-infrared (mid-IR) coherent sources will not only improve the performance of many existing applications, but also enable entirely new applications in the fields of spectroscopy, defence, sensing, polymer processing and medicine [1]–[6]. In particular the high energy region of the mid-IR, i.e. the 3–5 μm spectral range has received significant attention because it can be accessed using fluoride fibers and it covers several fundamental molecular bond absorption features, such as those of C-H, C-O, and N-H, which are key to sensing and materials processing. In addition, this spectral band overlaps with an exceptional atmospheric transmission window enabling new opportunities in, for example, light detection and ranging (LIDAR) and countermeasures against heat-seeking missiles [3], [7].

Manuscript received March 21, 2020; revised June 14, 2020; accepted June 15, 2020. Date of publication June 23, 2020; date of current version October 15, 2020. The work was supported by the Asian Office of Aerospace RD under Grant FA2386-19-1-0043. *(Corresponding author: Md Ziaul Amin.)*

Md. Ziaul Amin, Matthew R. Majewski, Robert I. Woodward, and Stuart D. Jackson are with MQ Photonics, School of Engineering, Macquarie University, Macquarie Park, NSW 2109, Australia (e-mail: md.ziaul.amin1@students.mq.edu.au; matthew.majewski@mq.edu.au; robert.woodward@mq.edu.au; stuart.jackson@mq.edu.au).

Alexander Fuerbach is with MQ Photonics, School of Engineering, Macquarie University, Macquarie Park, NSW 2109, Australia, and also with the MQ Photonics, Department of Physics and Astronomy, Macquarie University, Macquarie Park, NSW 2109, Australia (e-mail: alex.fuerbach@mq.edu.au).

Color versions of one or more of the figures in this article are available online at https://ieeexplore.ieee.org.

Digital Object Identifier 10.1109/JLT.2020.3004428

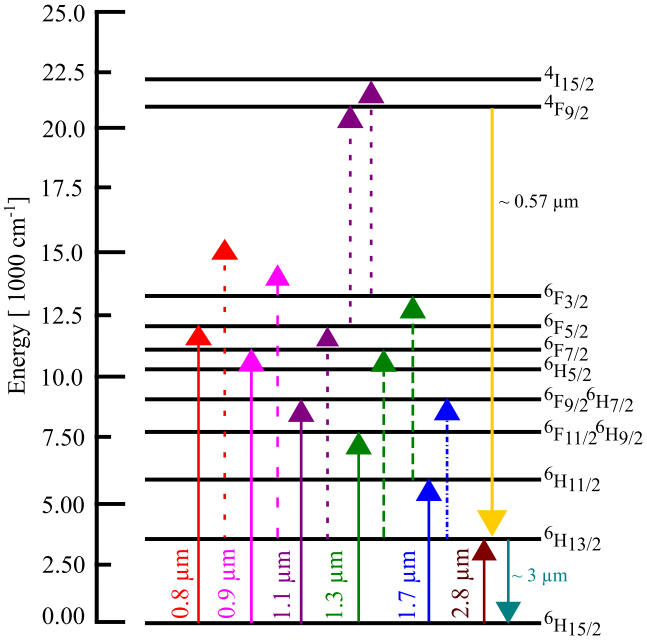

Fig. 1. Dy^{3+} energy level diagram showing pump excited state absorption (ESA) for 1.1 μm, 1.3 μm, and 1.7 μm. From the upper laser level of the 3 μm transition, there is no resonant energy level for 0.8 μm and 0.9 μm pumping wavelengths as presented by the red and pink dashed line, which is suited to avoid detrimental pump-ESA.

To date three rare-earth dopants: erbium (Er^{3+}), holmium (Ho^{3+}) and dysprosium (Dy^{3+}) have been reported to generate mid-IR laser emission. The emission spectrum of Er^{3+}:ZBLAN glass covers the 2.6–3.0 μm [8] and the 3.2–3.9 μm [9] spectral range. Ho^{3+}:ZBLAN glass can emit mid-IR radiation from 2.8–3.0 μm [10]. The fluorescence spectrum of the third dopant, Dy^{3+}, ranges from 2.6–3.4 μm, thus also covering the gap in the erbium emission. Moreover, a continuous wave (CW) tuning range of 600 nm, the widest for any rare-earth-doped fiber laser, was demonstrated from a Dy^{3+}-doped mid-IR fiber laser [11]. The Dy^{3+} energy level diagram, as shown in Fig. 1, depicts the ground state terminated 3 μm transition as well as several closely spaced levels above. As relaxation from all of the levels is dominated by rapid multiphonon decay in ZBLAN glass to the upper 3 μm laser level, there are several viable pumping options.

From the wide choice of possible pump wavelengths, a convenient 1.1 μm pump source ($^6H_{15/2}$ – $^6H_{7/2}$) was chosen for the first report of 3 μm laser output from a free running Dy^{3+}-doped fiber laser [12]. From that first report, 3 μm laser

output power was measured with 4.5% slope efficiency relative to absorbed pump power. In a follow-up report, an improved laser slope efficiency of 23% relative to absorbed pump power was reported by using an optimized 50% output coupler [13]. The use of 1.3 μm ($^6H_{15/2} - {}^6H_{9/2}$) pump wavelength reduces the quantum defect and should therefore increase the laser slope efficiency. However, it was found that the laser slope efficiency of 20% with respect to absorbed pump power was lower than that of the 1.1 μm pumped-system [14]. This was explained by the fact that pump excited state absorption (ESA) degrades the laser performance and limits the maximum laser slope efficiency to 49% (62%) and 39% (45%), with respect to launched pump power (with respect to absorbed pump power), of the Stokes limit of 1.1 μm and 1.3 μm pumped Dy^{3+}-doped mid-IR fiber lasers, respectively.

Recently, an increasing interest has been seen in exploiting the benefit of in-band 2.8 μm ($^6H_{15/2} - {}^6H_{13/2}$) pumping, which reduces the quantum defect and enabled an efficient Dy^{3+}-doped mid-IR fiber laser [15]. With in-band 2.8 μm pumping, a record slope efficiency of 73% (with respect to launched pump power) and 77% (with respect to absorbed pump power) has been reported from a Dy^{3+}-doped mid-IR fiber laser [16]. Very recently, an even higher slope efficiency record (91% relative to launched pump power) has been reported using this in-band pumping scheme in a Dy^{3+}-doped mid-IR fiber laser [17]. This new record has been achieved by using a low loss (0.05 dB/m) Dy^{3+}-doped ZBLAN fiber. In another report, a laser output power of 10.1 W with 58% slope efficiency (with respect to launched pump power) has been reported [18], which shows the power scaling potential of Dy^{3+}:ZBLAN fiber lasers.

While in-band pumping enabled the highest laser power and efficiency from Dy^{3+}-doped fiber lasers to date, this pumping scheme does not allow to access the full emission bandwidth of the Dy^{3+} ion. Moreover, high power laser diodes are not available for in-band pumping wavelengths, which is restricting the development of high-power diode pumped systems. Existing double-clad fibers with polymer coating are also not suitable for in-band pumped system. Therefore, there is a clear need to re-investigate the two remaining near-IR pump wavelengths (0.8 μm and 0.9 μm) to access a wider bandwidth (for ultrafast or widely tunable operation) and 4 μm emission of a Dy^{3+} ion as carried out in [7], [11]. Most importantly, these wavelengths are conveniently available from cost effective high power laser diodes (at least at 0.8 μm with output power of $\sim$100 W). Moreover, as Dy^{3+}'s energy level structure includes a large forbidden energy gap between the $^4F_{9/2}$ and $^6F_{3/2}$ levels (see Fig. 1), these new wavelengths are uniquely suited to avoid detrimental pump ESA. Hence our motivation for this work was to study 0.8 μm ($^6H_{15/2}$–$^6F_{5/2}$) and 0.9 μm ($^6H_{15/2}$–$^6F_{7/2}$) pumped Dy^{3+}-doped fiber lasers.

II. Absorption Cross-section Measurement of Dysprosium

As the 0.8 μm and 0.9 μm pump wavelengths are used for the first time in a Dy^{3+}-doped fiber laser, an accurate measurement of the Dy^{3+} absorption cross-section for both wavelengths is required to develop a numerical model that can predict the system performance with reasonable accuracy. The absorption cross-section data was measured from a Dy^{3+}-doped ZBLAN bulk glass sample using a Cary 5000 UV-Vis-NIR spectrophotometer. Two cubic shaped ZBLAN glass samples doped with 2 mol% and 1 mol% Dy^{3+} were used for measuring the absorption data which were then fitted by the following relations to calculate the absorption cross-section:

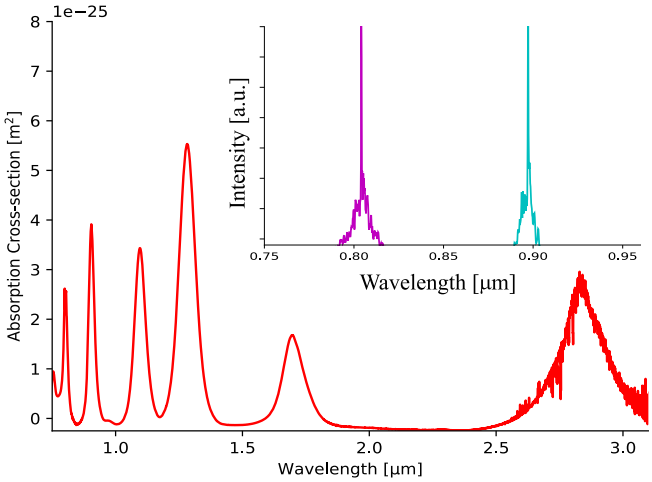

Fig. 2. Dy^{3+} absorption cross-section measured from bulk ZBLAN glass sample. In the inset, the emission spectrum of a titanium-sapphire laser is shown for a center wavelength of 0.8 μm and 0.9 μm, respectively.

$$\alpha_{abs1} = N\sigma(\lambda)l_1 + B(\lambda) \quad (1)$$

$$\alpha_{abs2} = 2N\sigma(\lambda)l_2 + B(\lambda) \quad (2)$$

where, α_{abs}, N, $\sigma(\lambda)$, and $B(\lambda)$ represent the absorption coefficient, number of dopant ions / mol%, absorption cross-section, and background loss for ZBLAN glass, respectively. The sample thickness for 1 mol% and 2 mol% were $l_1 = 13.15$ mm, and $l_2 = 11.98$ mm, respectively. The background loss, represented by $B(\lambda)$, was subtracted to calculate the Dy^{3+} absorption cross-section, as shown in Fig. 2. The calculated peak absorption cross-sections of the Dy^{3+} ion are 2.6×10^{-25} m^2 and 3.9×10^{-25} m^2 for 0.8 μm and 0.9 μm pump wavelengths, respectively. Previously, the absorption data of a Dy^{3+} in ZBLAN glass was reported in terms of the absorption coefficient [19]. In their measurement, they did not mention the impact of intrinsic ZBLAN glass absorption. For comparison, we have converted their measured absorption coefficient to absorption cross-section data and found that the peak values at 0.8 μm and 0.9 μm are 3×10^{-25} m^2, and 4×10^{-25} m^2, respectively. These peak values are comparatively higher than what we have measured using our background subtraction method, which might arise from intrinsic ZBLAN glass absorption.

III. Experimental Setup

In our experiment, we have used a single-clad (SC) Dy^{3+}-doped ZBLAN fiber (Le Verre Fluoré, France) with 0.2 mol% dopant concentration, which has also been used in a number

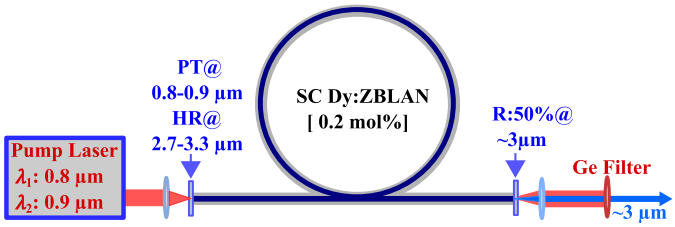

Fig. 3. A Dy^{3+}-doped mid-IR fiber laser. The pumping end of the fiber is butt-coupled to a mirror which is highly reflective (HR) from 2.7-3.3 μm and partially transmissive (PT) at both pump wavelengths, 80% at 0.8 μm and 73% at 0.9 μm (adapted from Ref. [20]).

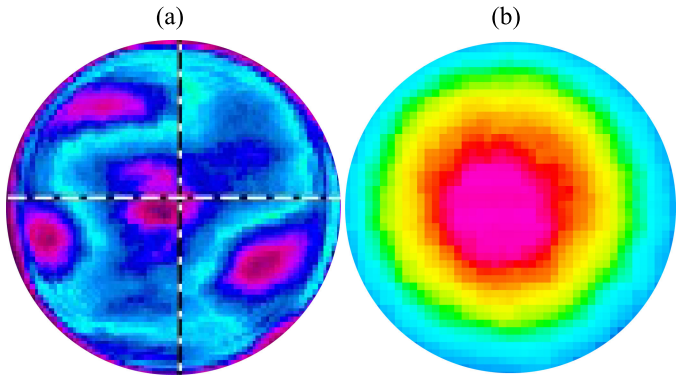

Fig. 4. (a) Image of collimated residual pump beam at 0.8 μm (b) image of collimated mid-IR laser beam.

of previous laser demonstrations [11], [15], [16]. The numerical aperture (NA) and core diameter of the fiber are 0.16 and 12.5 μm, respectively, which ensure single-mode operation down to 2.6 μm. However, the fiber is multi-mode for both pump wavelengths (0.8 μm and 0.9 μm), which can thus excite higher-orders modes in the fiber core. A tunable titanium-sapphire laser was utilized to generate pump light at both 0.8 μm and 0.9 μm. The pump spectrum at both wavelengths is shown in the inset of Fig. 2. The pump was focused into the Dy^{3+}-doped fiber with an anti-reflection-coated aspherical lens (focal length = 12 mm) with 77% launch efficiency. The fiber output was collimated using an uncoated CaF_2 lens (focal length = 20 mm).

In our initial experiment, we focused on characterising the multi-mode nature of the fiber at both pump wavelengths, which was done in absence of cavity mirrors. The collimated residual pump beam was then imaged onto a Pyrocam IV beam profiling camera to investigate the higher-order mode excitation in the Dy^{3+}-doped fiber core. Further, the residual pump power after the 0.5 m Dy^{3+}-doped fiber was recorded for investigating any potential higher-order energy transfer mechanisms or pump ESA.

For demonstration of lasing, we utilized bulk mirrors butt-coupled to both fiber ends, as shown in Fig. 3. At the input (pumping) end, the butt-coupled mirror was highly reflective (HR), approximately 99% from 2.7–3.3 μm and partially transmissive (PT), approximately 80% at 0.8 μm and 73% at 0.9 μm. At the output end, a broadband 50% reflective mirror at 3 μm was butt-coupled and used as an output-coupler. A germanium (Ge) filter was employed to separate laser signal from residual pump light. The laser output powers were measured using a thermal power meter and then corrected to account for losses introduced by the Ge filter and lens reflections.

IV. Fiber Multi-mode Impact on Pump Absorption

As we expect the multi-mode nature of the pump to affect the laser performance to some degree, we analyzed the mode-profile of the collimated residual pump beam as shown in Fig. 4 (a). The residual pump power image confirms higher-order modes excitation in the fiber core. For comparison, we have also imaged the mid-IR laser output (see Fig. 4 (b)), which emits as a pure LP_{01} mode as expected.

In a second step of our investigation, we measured the residual pump power as a function of launched pump power of a 0.5 m Dy^{3+}-doped fiber to investigate any unforeseen pump ESA or other detrimental energy transfer mechanisms. We expect that if present, these effects would manifest in increased pump absorption, as previous work has shown that such ESA processes are required to match experimental and numerical results [11]. Moreover, pump ESA processes at 1.1 μm pumping wavelength exhibited visible light emission from a Dy^{3+}-doped ZBLAN fiber [12]. However, we did not observe any visible light emission from a Dy^{3+}-doped ZBLAN fiber for 0.8 μm and 0.9 μm pumping wavelengths. If there were a presence of any unforeseen pump ESA or higher-order energy transfer mechanisms for these wavelengths, pump absorption is expected to be higher than the calculated value. However, the comparison

TABLE I
Simulation Parameters for the Dy^{3+}-doped Fiber Laser

Parameter	Symbol	Value
Doping concentration (m^{-3})	N_t	3.66×10^{25}
Branching ratios [24], [25]	β_{10}, β_{21}, β_{20}, β_{32}, β_{31}, β_{30}, β_{42}, β_{41}, β_{40}, β_{54}, β_{53}, β_{52}, β_{51}, β_{50}, β_{63}, β_{62}, β_{61}, β_{60}, β_{74}, β_{73}, β_{72}, β_{71}, β_{70}, β_{84}, β_{83}, β_{82}, β_{81}, β_{80}	1, 0.052, 0.948, 0.01, 0.15, 0.84, 0.03, 0.23, 0.74, 0.02, 0.11, 0.47, 0.34, 0.06, 0.02, 0.08, 0.06, 0.84, 0.02, 0.05, 0.07, 0.24, 0.62, 0.02, 0.11, 0.07, 0.57, 0.23
Radiative lifetime (ms) [24], [25]	$\tau_{r,1}$, $\tau_{r,2}$, $\tau_{r,3}$, $\tau_{r,4}$, $\tau_{r,5}$, $\tau_{r,6}$, $\tau_{r,7}$	46.8, 13.7, 5.2, 3.5, 20.2, 1.3, 1
Non-radiative lifetime (µs) [24]	$\tau_{nr,1}$, $\tau_{nr,2}$, $\tau_{nr,3}$, $\tau_{nr,4}$, $\tau_{nr,5}$, $\tau_{nr,6}$, $\tau_{nr,7}$,	650, 1.25, 0.1, 0.006, 0.152, 0.009, 0.0003
Fiber background loss (dB/m)	$l(\lambda)$	0.3
Pump wavelengths (µm)	λ_{p1}, λ_{p2}	0.8, 0.9
Absorption cross-section (m^2) at 0.8 µm	σ_{07}	2.6×10^{-25}
Absorption cross-section (m^2) at 0.9 µm	σ_{06}	3.1×10^{-25}
Emission cross-section (m^2)	σ_{10}	2.6×10^{-25}
Overlap factor (pump)	λ_{p1}, λ_{p2}	0.87, 0.93
Overlap factor (signal)	λ_s	0.76
Front mirror reflectively	$R_f(\lambda_p)$, $R_f(\lambda_s)$	0%, 99%
Back mirror reflectively	$R_b(\lambda_p)$, $R_b(\lambda_s)$	50%, 50%

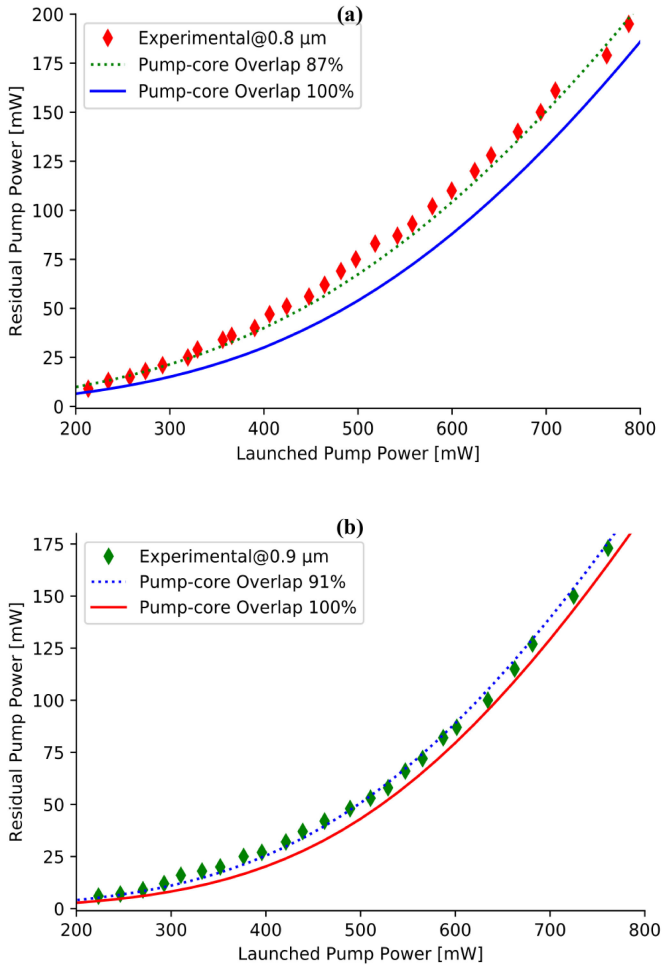

Fig. 5. Residual pump power for 0.5 m Dy^{3+}-doped fiber as a function of launched pump power for (a) 0.8 μm and (b) 0.9 μm pump wavelengths, respectively (adapted from Ref. [20]).

of experimental data and simulation results (relevant simulation parameters are given in Table. I) indicates reduced pump absorption, as seen in Fig. 5.

To find the cause of reduced pump absorption at 0.8 μm and 0.9 μm pumping wavelengths, we theoretically calculate the effect of multi-mode behaviour on pump absorption. For this, we have calculated the number of supported modes in the fiber assuming a weakly guiding approximation, where the index difference between core (n_{core}) and cladding (n_{clad}) is small. Under this assumption, the number of supported modes in the fiber can be calculated by using the following eigenvalue equation [21]:

$$U\frac{J_{l-1}(U)}{J_l(U)} = -W\frac{K_{l-1}(U)}{K_l(U)} \tag{3}$$

where $U = a\sqrt{k_0^2 n_{core}^2 - \beta^2}$, $W = a\sqrt{\beta^2 - k_0^2 n_{clad}^2}$. In the above relations, a, J, and K define fiber core radius, ordinary Bessel function of the first kind, and modified Bessel function of the second kind, respectively.

To find the propagation constant β of the supported modes, the parameter $V = a\sqrt{k_0^2 n_{core}^2 - k_0^2 n_{clad}^2}$ should satisfy the

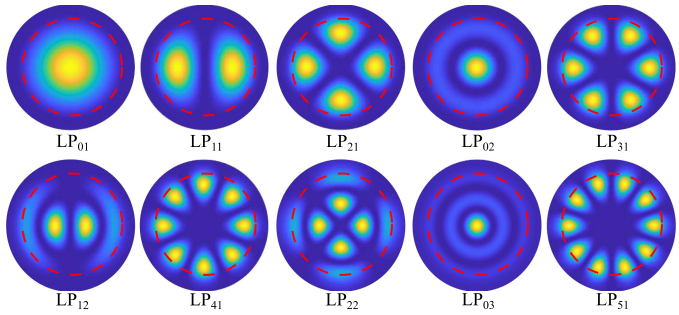

Fig. 6. Number of LP_{lm} modes supported by Dy^{3+}-doped fiber at 0.8 μm, where core is identified with a dashed line.

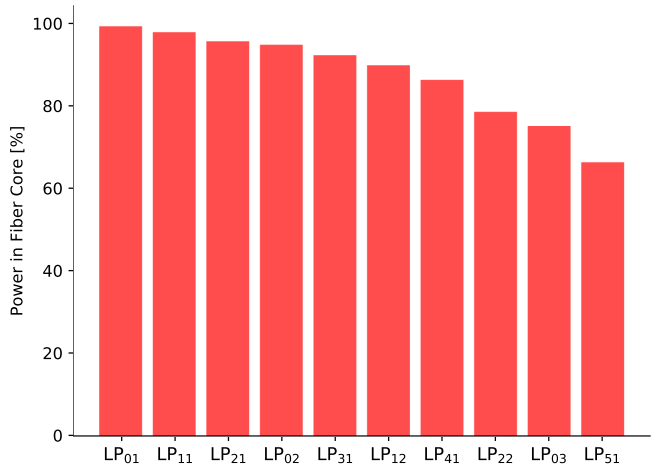

Fig. 7. Fraction of core power for different fiber modes.

following relation:

$$V^2 = U^2 + W^2 \tag{4}$$

where $k_0 = \frac{2\pi}{\lambda}$.

For a given l index there will be m solutions of the eigenvalue equation (3), where each solution is known as a linearly polarized LP_{lm} mode. For the Dy^{3+}-doped fiber used, there exist ten (10) guided LP_{lm} modes for 0.8 μm pumping wavelength, as shown in Fig. 6. The degree of excitation of higher-order guided modes influences the pump power confinement in the fiber core. As the degree of excitation of higher-order guided modes increases, the fraction of pump power confined in the fiber core decreases. The pump power confinement (η) in the fiber core for each mode is calculated by the following relation [22]:

$$\eta = \frac{U^2}{V^2}\left(\frac{W^2}{U^2} + \frac{K_0^2}{K_1^2}\right) \tag{5}$$

The calculated fractional pump power confined in the fiber core as a function of fiber pump modes is shown in Fig. 7. Assuming equal excitation of all modes for 0.8 μm, the average pump power confined to the fiber core is about 88% of the launched pump power. Moreover, higher-order modes excitation in the doped fiber reduces the pump-core overlap, which consequently decreases the pump-signal conversion efficiency. The analysis done for 0.8 μm pumping wavelength is also true for 0.9 μm pump wavelength as the Dy^{3+}-doped fiber is still multi-mode

for this wavelength. For longer 0.9 μm pump wavelength, the fraction of core power will decrease for each mode. Considering the closeness of these two pump wavelengths, we assume the same fractional core power for each mode as calculated for 0.8 μm pump wavelength. Based on this assumption, we have calculated the average pump power confinement for 0.9 μm wavelength. In this pumping case, the number of supported LP_{lm} modes reduces to seven (7), which consequently increases the average pump power confinement in the fiber core to 93%. The pump absorption in the Dy^{3+}-doped fiber is simulated by changing the overlap between pump and core. The experimental results show good agreement with the numerical simulation data, as shown in Fig. 5.

V. Rate Equation Modelling

Development of a reliable numerical model as a supplement of an experimental demonstration is important, which can provide a deeper understanding of the behavior of the system than an experimental demonstration alone. We have therefore developed a numerical model to predict the experimental laser behaviour with identical cavity components as described in our experimental setup. Here, we are only interested in simulating continuous wave (CW) laser behaviour, which allows us to ignore temporal dependence of pump and signal power evolution along the Dy^{3+}-doped fiber and consider only steady solution of equation (7). This is done by setting equation (7) equal to zero. The spatial dependence of pump and signal power in the Dy^{3+}-doped fiber are calculated by solving the power flow equation:

$$\frac{dP^{\pm}(\lambda,z)}{dz} = \pm P^{\pm}(\lambda,z) \times \left[\Gamma(\lambda)\left(\sum_{ij}\sigma_{ij}(\lambda)N_i(z) - \sigma_{ji}(\lambda)N_j(z)\right) - l(\lambda)\right] \tag{6}$$

Where $\Gamma(\lambda)$, and $l(\lambda)$ are the core overlap factor, and background loss for each spectral channel (pump and signal), respectively. The σ_{ij} term represents cross section of transition between i to j levels with population N_i and N_j. When $i < j$ this indicates absorption and when $i > j$ it indicates emission. Sum is taken over for all possible pair combinations (i, j) with up to $m \times (m-1)$ possible terms, where m is the number of energy level.

Power flow equation requires population densities along the fiber, which can be found by solving rate equations as described by (7). Laser active ions doped in the low phonon energy glass host result in a complex energy level structure with several long lived states, which requires a consideration of large number of transitions. This complex rate equation system can be represented in a matrix notation, which brings generality and can be adaptable to any rate equations system [23]. The atomic level populations for m energy levels and their respective rate equations are presented in the following general equation:

$$\frac{d\mathbf{N}}{dt} = \mathbf{L}\mathbf{N} \tag{7}$$

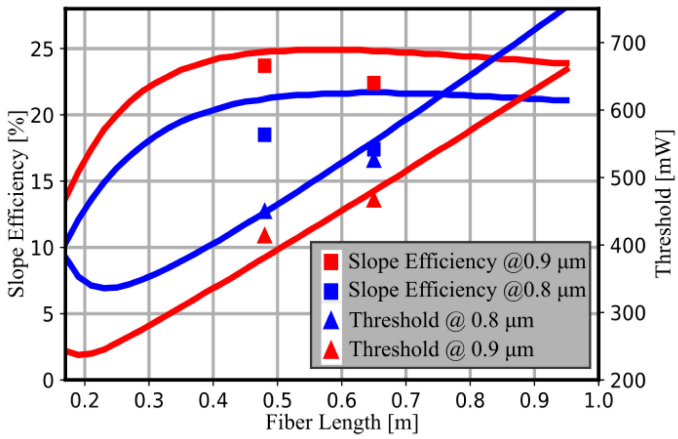

Fig. 8. Comparison of experimental and simulated laser slope efficiency (relative to launched pump power) and threshold for 0.8 μm and 0.9 μm pump wavelengths. The blue and red solid line represent the simulated laser behaviour for 0.8 μm and 0.9 μm pump wavelengths, respectively. Measured slope efficiencies and thresholds are presented by square and triangular symbols, respectively.

Where, $\mathbf{L}$ defines the linear population rate change matrix comprising of spontaneous emission, multi-phonon relaxation, and stimulated absorption or emission terms. Here, the $\mathbf{L}$ is presented in the matrix form:

$$\mathbf{L} = \begin{bmatrix} -\sum_{i=0}^{(m-1)} R_{0i} & \cdots & R_{(m-1)0} \\ \vdots & \ddots & \vdots \\ R_{0(m-1)} & \cdots & -\sum_{i=0}^{(m-1)} R_{(m-1)i} \end{bmatrix} \tag{8}$$

We consider the ground level as 0 level. Therefore, the $(m-1)$ level represents the highest energy level. The incoming (positive) rate changes to the population N_i from all individual levels $(i \neq j)$ are represented by non-diagonal elements, while diagonal elements contain all outgoing (negative) rate changes. These outgoing rate changes comprise of $\beta_{ij}/\tau_{r,i}$, non-raditive decay rates (R_{ij}^{nr}), and stimulated absorption or emission rates $[\sum_{\lambda}\sigma_{ij}(\lambda)\frac{P(\lambda)\Gamma(\lambda)}{A(hc/\lambda)}]$ for the $i \rightarrow j$ transitions, which is summed over for all spectral channels and both propagation directions. Here, β_{ij}, $\tau_{r,i}$, and A are branching ratio, radiative lifetime, and fiber core area, respectively. Parameters used in our numerical simulations are given in Table. I.

VI. Results

Initially, the dependence of laser slope efficiency and threshold pump power as a function of Dy^{3+}-doped fiber length was simulated, which gave us an indication of the optimum fiber length to choose for our laser experiment. The simulated laser slope efficiency and threshold as a function of Dy^{3+}-doped fiber length is shown in Fig. 8. The Dy^{3+}-doped fiber background loss was previously measured to be 0.3 dB/m at 3.39 μm and this value was used in our simulations [16]. For this background loss, the laser slope efficiency reduces from 26.6% to 22.1% and from 30.3% to 25.2% for 0.8 μm and 0.9 μm, respectively, compared to the case of a lossless fiber. The fiber multi-mode

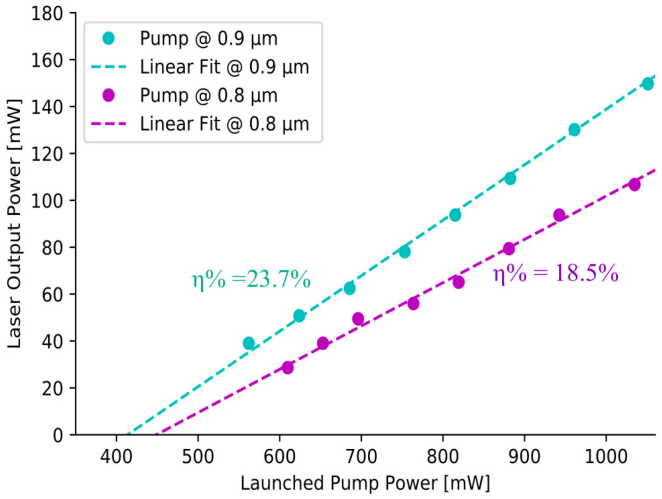

Fig. 9. Laser output power as a function of launched pump power for 0.48 m Dy^{3+}-doped fiber, which produces laser slope efficiency of 23.7% and 18.5% for 0.8 μm and 0.9 μm pumping wavelengths, respectively (adapted from Ref. [20]).

impact on laser performance was simulated by varying the pump-core overlap factor to 87% and 93% for 0.8 μm and 0.9 μm pumping, respectively. For this multi-mode impact, the laser slope efficiencies further reduce from 22.1% to 21.7% (for 0.8 μm) and from 25.7% to 24.9% (for 0.9 μm). The simulated laser slope efficiency is maximum for a length of around 0.5 m of Dy^{3+}-doped fiber. Based on the simulation results, we have used two different Dy^{3+}-doped fiber lengths (0.48 m, and 0.62 m) as the laser gain medium. As expected, the maximum laser slope efficiency was measured for 0.48 m of Dy^{3+}-doped fiber, as shown in Fig. 9.

As the incident pump power was increased, lasing was observed at 449 mW and 413 mW of launched pump power for 0.48 m of Dy^{3+} fiber for 0.8 μm and 0.9 μm pump wavelengths, respectively. The maximum experimental slope efficiency for 0.8 μm and 0.9 μm pumped Dy^{3+}-doped fiber laser is 18.5% and 23.7% with respect to launched pump power, respectively. Similarly, the laser slope efficiencies and thresholds are measured for 0.62 m of Dy^{3+}-doped fiber. With the increase of Dy^{3+}-doped fiber length to 0.62 m, the laser slope efficiencies decrease to 17.4% and 22.4% and lasing thresholds increase to 525 mW and 466 mW for 0.8 μm and 0.9 μm excitation wavelengths, respectively.

The lasing spectrum was also recorded for the two different Dy^{3+}-doped fiber lengths and is shown in Fig. 10. The Dy^{3+}-doped mid-IR fiber laser is a ground-state terminated three-level system. With uni-directional pumping, length-averaged population inversion decreases with increasing Dy^{3+}-doped fiber length. Therefore, when the Dy^{3+}-doped fiber length is increased, shorter signal wavelengths are reabsorbed, which red-shifts the lasing wavelength.

The experimental laser slope efficiencies and thresholds are superimposed in Fig. 8 to compare with the simulation results. The experimental results follow a similar trend as expected from the numerical simulation. In our simulation, we have found

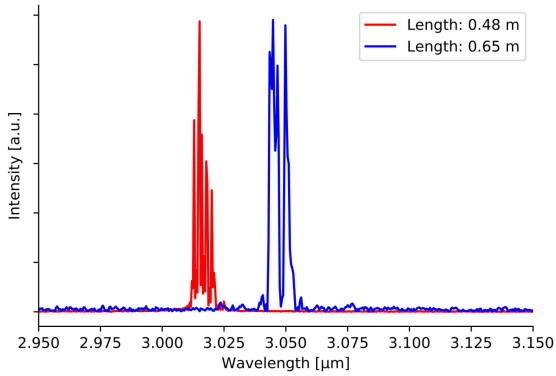

Fig. 10. Laser spectrum for 0.48 m and 0.62 m of Dy^{3+}-doped fiber (adapted from Ref. [20]).

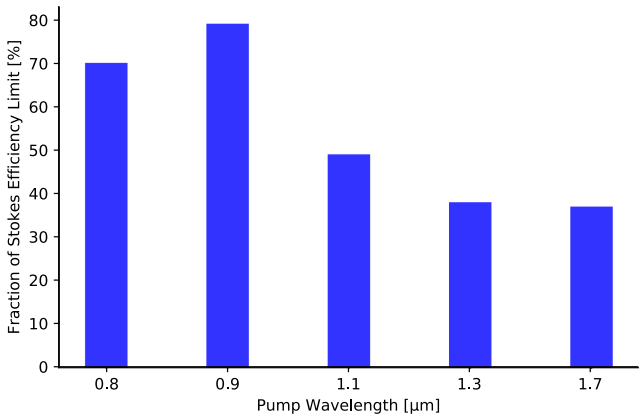

Fig. 11. Fractional Stokes efficiency limit comparison of all near-IR pumped Dy^{3+}-doped mid-IR fiber lasers [11], [14], and [26].

that fiber background loss (0.3 dB/m) reduced the laser slope efficiency to 83% of the Stokes limit for both 0.8 μm and 0.9 μm pump wavelengths. In addition, fiber multi-mode behaviour reduces effective pump absorption in the fiber core, which consequently reduces the laser slope efficiency. The cumulative effect of fiber background loss and fiber multi-mode effect reduces the laser slope efficiencies to 81% and 82% of Stokes limit for 0.8 μm and 0.9 μm pumping wavelengths, respectively.

To select a suitable near-IR excitation wavelength for Dy^{3+}-doped fiber lasers, we have compared the performance of all near-IR pumped demonstrations, as shown in Fig. 11. To date, three near-IR pump wavelengths, 1.1 μm [12], [26], 1.3 μm [14], and 1.7 μm [11] have been reported for Dy^{3+} doped mid-IR fiber lasers with a maximum slope efficiency of 18%, 16.5%, and 21%, respectively. In our demonstrations, we recorded a maximum slope efficiency of 18.5% and 23.7% for 0.8 μm, and 0.9 μm pumping wavelengths, respectively. Among all near-IR pumped Dy^{3+}-doped fiber lasers, laser slope efficiency reaches the highest value for 0.9 μm pumping wavelength. Moreover, the laser slope efficiency for 0.8 μm is almost comparable to 1.1 μm and 1.7 μm pumping cases. The laser slope efficiency of all previous near-IR pumped system is limited by the detrimental pump ESA and reaches up-to 49% of the Stokes limit for 1.1 μm excitation wavelength. In our recent demonstrations, the laser slope efficiency reaches the maximum 79% of the Stokes efficiency limit

at 0.9 μm. This performance metric decreases to 70% for 0.8 μm pumping wavelength. The causes of still lower slope efficiency than Stokes efficiency limit are identified as fiber background loss and fiber multi-mode behaviour at both pump wavelengths. Higher fractional slope efficiency is possible by reducing the fiber background loss for both pump wavelengths. Moreover, these wavelengths can be generated from available high power laser diodes (with output power of $\sim$100 W, and $\sim$8 W at 0.8 μm and 0.9 μm, respectively) and used to access the entire emission range of Dy^{3+} including 4 μm as demonstrated in [11], and [7].

The important features of these new excitation wavelengths motivate us to design a double-clad Dy^{3+}-doped fiber with an aim to develop a cladding-pumped system, which can be pumped with a high-power laser diode. In the cladding-pumped system, the effective pump-core overlap is smaller than the core-pumped system, which reduces the effective pump absorption. The reduction in pump absorption can be simply calculated by using the core to cladding area ratio. To increase the effective pump absorption, dopant concentration, fiber length or combination of both can be increased, as has been demonstrated in Er^{3+} and Ho^{3+} based 3 μm laser systems. In both Er^{3+} and Ho^{3+} based systems, the laser transition terminates in an excited state, which can rapidly depopulate. Therefore, signal re-absorption probability in Er^{3+} and Ho^{3+} based 3 μm laser system decreases. On the other hand, the 3 μm laser transition of Dy^{3+} is a ground state terminated true three level system. In the Dy^{3+}-based system, there is significant population in the ground state, therefore, signal re-absorption cannot be avoided even under strong pumping condition. Moreover, the product of emission cross-section (2.6×10^{-25} m^2) and excited state lifetime ($\sim$650 μs), which is inversely proportional to the threshold, for a Dy^{3+} ion is smaller than that of Er^{3+} and Ho^{3+} ions. Therefore, inherently Dy^{3+}-doped mid-IR fiber lasers have a higher threshold than Er^{3+} and Ho^{3+} based 3 μm laser for a similar cavity arrangement.

Considering this issue, we have designed a double-clad Dy^{3+}-doped fiber by varying the dopant concentration and core-cladding ratio so that a diode-pumped Dy^{3+}-doped mid-IR fiber laser can be developed in the near future with a reasonable threshold pump power. In our fiber design, we choose the core diameter and numerical aperture as 15 μm and 0.14, respectively. These parameter ensure single mode operation down to 2.74 μm. Subsequently, we have numerically simulated the laser slope efficiencies and thresholds as a function of Dy^{3+} concentration and cladding diameter. In our simulation, we have considered 0.9 μm pumping wavelength, 0.05 dB/m fiber background loss (taken from [17]), 99.99% and 50% reflective mirrors in the pumping end and output-coupler, respectively. For each doping concentration and cladding diameter, we have numerically calculated the laser slope efficiency and threshold as a function of Dy^{3+}-doped fiber length. The calculated maximum slope efficiency and corresponding threshold values for different doping concentration are presented in Table II. From the numerical simulation, it is found that a diode-pumped Dy^{3+}-doped fiber laser can be developed in the near future with a sub 10 W level lasing threshold.

TABLE II
SLOPE EFFICIENCY AND THRESHOLD SIMULATIONS OF A Dy^{3+}-DOPED MID-IR FIBER LASER AS A FUNCTION OF CLADDING DIAMETER AND DY ION CONCENTRATION

Cladding diameter	Concentration	Threshold	Slope Efficiency
125 μm	1 mol %	7.35 W	23.17%
	2 mol %	7.43 W	22.96%
	3 mol %	7.50 W	22.72%
130 μm	1 mol %	8.31 W	24.80%
	2 mol %	8.35 W	24.70%
	3 mol %	8.39 W	24.53%
135 μm	1 mol %	9.40 W	25.38%
	2 mol %	9.42 W	25.32%
	3 mol %	9.45 W	25.24%

VII. CONCLUSION

In summary, we have identified two new near-IR pump wavelengths (0.8 μm and 0.9 μm) for Dy^{3+}-doped mid-IR fiber lasers for the the first time to the best of our knowledge. No detrimental pump ESA and higher energy transfer mechanisms are observed for these pump wavelengths. This claim is validated with a numerical model by analysing the residual pump power of a 0.5 m Dy^{3+}-doped fiber and is also supported by the Dy^{3+}-energy level diagram. Although there is no higher energy transfer mechanism, the maximum measured laser slope efficiencies are 70% and 79% (which is the highest among all near-IR pumped Dy^{3+}-doped mid-IR fiber laser) of the Stokes limit for 0.8 μm and 0.9 μm excitation wavelengths, respectively. The cause of the lower slope efficiencies are identified as the fiber background loss (0.3 dB/m measured at 3.39 μm) and multi-mode behaviour of Dy^{3+}-doped fiber at these pump wavelengths. The slope efficiency of Dy^{3+}-doped ZBLAN fiber lasers would improve in the near future by using a low loss fiber. Moreover, a suitable double-clad fiber design would help to realize a compact and cost-effective diode-pumped Dy^{3+}-doped mid-IR fiber laser using these ESA free pump wavelengths.

REFERENCES

[1] F. K. Tittel, D. Richter, and A. Fried, *Mid-Infrared laser applications in spectroscopy*. Berlin, Germany: Springer, 2003, pp. 458–529.
[2] A. Sijan, "Development of military lasers for optical countermeasures in the mid-IR," in *Proc. Technol. Opt. Countermeasures. VI.*, Sep. 2009, vol. 7483, Art. no. 748304.
[3] R. I. Woodward, M. R. Majewski, D. D. Hudson, and S. D. Jackson, "Swept-wavelength mid-infrared fiber laser for real-time ammonia gas sensing," *APL Photon.*, vol. 4, no. 2, 2019, Art. no. 020801.
[4] A. R. Adams *et al.*, "Mid-infrared laser applications in medicine and biology," *Philos. Trans. Royal. Soc. London. Series. A: Math., Physical. Eng. Sci.*, vol. 359, no. 1780, pp. 635–644, 2001.
[5] M. F. Pereira, *Terahertz and Mid Infrared Radiation: Detection of Explosives and CBRN (Using Terahertz)*, (NATO Science for Peace and Security Series B: Physics and Biophysics Series), Mauro F. Pereira and Oleksiy Shulika, Eds., Berlin, Germany: Springer, 2014.
[6] C. Frayssinous, V. Fortin, J.-P. Brub, A. Fraser, and R. Valle, "Resonant polymer ablation using a compact 3.44 μm fiber laser," *J. Mater. Process. Technol.*, vol. 252, pp. 813–820, 2018.
[7] M. R. Majewski, R. I. Woodward, J.-Y. Carreé, S. Poulain, M. Poulain, and S. D. Jackson, "Emission beyond 4 μm and mid-infrared lasing in a dysprosium-doped indium fluoride (InF_3) fiber," *Opt. Lett.*, vol. 43, no. 8, pp. 1926–1929, Apr. 2018.
[8] F. Auzel, D. Meichenin, and H. Poignant, "Laser cross-section and quantum yield of Er^{3+} at 2.7 μm in a ZrF_4-based fluoride glass," *Electron. Lett.*, vol. 24, no. 15, pp. 909–910, Jul. 1988.

[9] O. Henderson-Sapir, S. D. Jackson, and D. J. Ottaway, "Versatile and widely tunable mid-infrared erbium doped ZBLAN fiber laser," *Opt. Lett.*, vol. 41, no. 7, pp. 1676–1679, Apr. 2016.
[10] L. Wetenkamp, G. West, and H. Tbben, "Optical properties of rare earth-doped ZBLAN glasses," *J. Non-Crystalline Solids*, vol. 140, pp. 35–40, 1992.
[11] M. R. Majewski, R. I. Woodward, and S. D. Jackson, "Dysprosium-doped ZBLAN fiber laser tunable from 2.8 μm to 3.4 μm, pumped at 1.7 μm," *Opt. Lett.*, vol. 43, no. 5, pp. 971–974, Mar. 2018.
[12] S. D. Jackson, "Continuous wave 2.9 μm dysprosium-doped fluoride fiber laser," *Appl. Phys. Lett.*, vol. 83, no. 7, pp. 1316–1318, 2003.
[13] Y. Tsang and A. El-Taher, "Efficient lasing at near 3 μm by a Dy-doped ZBLAN fiber laser pumped at 1.1 μm by an Yb fiber laser," *Laser Phys. Lett.*, vol. 8, no. 11, pp. 818–822, 2011.
[14] Y. H. Tsang, A. E. El-Taher, T. A. King, and S. D. Jackson, "Efficient 2.96 μm dysprosium-doped fluoride fibre laser pumped with a Nd:YAG laser operating at 1.3 μm," *Opt. Express*, vol. 14, no. 2, pp. 678–685, Jan. 2006.
[15] M. R. Majewski and S. D. Jackson, "Highly efficient mid-infrared dysprosium fiber laser," *Opt. Lett.*, vol. 41, no. 10, pp. 2173–2176, May 2016.
[16] R. I. Woodward, M. R. Majewski, G. Bharathan, D. D. Hudson, A. Fuerbach, and S. D. Jackson, "Watt-level dysprosium fiber laser at 3.15 μm with 73% slope efficiency," *Opt. Lett.*, vol. 43, no. 7, pp. 1471–1474, Apr. 2018.
[17] M. R. Majewski, M. Z. Amin, T. Berthelot, and S. D. Jackson, "Directly diode-pumped mid-infrared dysprosium fiber laser," *Opt. Lett.*, vol. 44, no. 22, pp. 3–6, 2019.
[18] V. Fortin, F. Jobin, M. Larose, M. Bernier, and R. Vallée, "10-W-level monolithic dysprosium-doped fiber laser at 3.24 μm," *Opt. Lett.*, vol. 44, no. 3, pp. 491–494, Feb. 2019.
[19] R. Piramidowicz, M. Klimczak, and M. Malinowski, "Short-wavelength emission analysis in Dy:ZBLAN glasses," *Opt. Mater.*, vol. 30, no. 5, pp. 707–710, 2008.
[20] M. Z. Amin, M. R. Majewski, R. I. Woodward, A. Fuerbach, and S. D. Jackson, "New excitation wavelengths for dysprosium-doped mid-infrared fiber lasers," in *Fiber Lasers XVII: Technology and Systems*, vol. 11260, Bellingham, WA, USA: SPIE, 2020, pp. 227–233.
[21] D. Gloge, "Weakly guiding fibers," *Appl. Opt.*, vol. 10, no. 10, pp. 2252–2258, Oct. 1971.
[22] A. W. Snyder, *Optical Waveguide Theory*, (Science paperbacks; 190 Series), Allan W. Snyder and John D. Love, Eds., London, U.K.: Chapman and Hall, 1983.
[23] R. I. Woodward and M. Gorjan, "Modelling mid-IR fibre laser systems," in *Mid-Infrared Fiber Photonics*, S. D. Jackson, M. Bernier, and R. Vallee, Eds. Cambridge, U.K.:Elsevier.
[24] L. Gomes, A. F. H. Librantz, and S. D. Jackson, "Energy level decay and excited state absorption processes in dysprosium-doped fluoride glass," *J. Appl. Phys.*, vol. 107, no. 5, 2010, Art. no. 053103.
[25] A. Tkachuk *et al.*, "Comparative spectroscopic study of the Dy^{3+} doped double chloride and double fluoride crystals for telecommunication amplifiers and IR lasers," *Acta Physica Polonica A*, vol. 95, no. 3, pp. 381–394, 1999.
[26] L. Sójka *et al.*, "Experimental investigation of mid-infrared laser action from Dy^{3+}-doped fluorozirconate fiber," *IEEE Photon. Technol. Lett.*, vol. 30, no. 12, pp. 1083–1086, Jun. 2018.

Md. Ziaul Amin received the B.Sc. degree in electronics and communication engineering from Khulna University, Bangladesh. In 2016, he received the master's degree in electrical engineering from the King Fahd University of Petroleum and Minerals (Saudi Arabia). Currently, he is a Ph.D. student with the School of Engineering at Macquarie University, Australia. His current research interests include doped fiber lasers and amplifiers.

Matthew R. Majewski received the M.S. degree from Northeastern University in 2012. Prior to joining Macquarie University in 2014 he was a member of the high power laser development team at Silex Systems, Australia. He completed his Ph.D. thesis on dysprosium mid-infrared fiber lasers in 2017 and is currently a Research Fellow with the Mid-infrared Fiber Sources Group. His current research focus is on the development of novel high power and ultrafast fiber laser sources.

Robert I. Woodward received the M.Eng. degree from Trinity Hall, University of Cambridge, U.K., in 2012, followed by a Ph.D. in laser physics & nonlinear fiber optics from Imperial College, London, U.K. He moved to Macquarie University, Australia, in 2016 to take up an MQ Research Fellowship to continue his fiber laser research, with a particular focus on the mid-infrared region.

Alexander Fuerbach was born in Vienna, Austria. He received the master's degree in engineering in 1999 and the Ph.D. degree in photonics in 2001 from the Vienna University of Technology under the supervision of Prof. Ferenc Krausz. He then joined Femtolasers Produktions GmbH where he was responsible for the development of advanced ultrashort-pulsed Ti:Sapphire laser systems. In 2004 he returned to academia and moved to Australia to take the position of a Research Fellow at the University of Sydney, studying ultrafast pulse propagation effects in novel optical fibres. In late 2005 he was awarded an Australian Postdoctoral Fellowship which allowed him to establish his own research group at Macquarie University in Sydney where he has been ever since. He is currently an Associate Professor and Higher Degree Research Director within the department of Physics and Astronomy. His principal research interests are focused on the interaction of femtosecond laser pulses with solid matter for photonic device fabrication and the development of waveguide and fibre laser systems, particular in the mid-infrared spectral region.

Stuart D. Jackson is a Professor with the School of Engineering, Macquarie University. He received the B.Sc.(Hons.) degree in 1989 from the University of Newcastle, Australia. In 1990, he joined the Centre for Lasers and Applications at Macquarie University to undertake research toward the Ph.D. degree. In 1995, he joined the Laser Photonics Group at the University of Manchester and initiated the research there into high power fibre lasers. Later in 1999, he returned to Australia and joined the Optical Fibre Technology Centre (OFTC) at the University of Sydney where he became a Senior Research Fellow and Technical Manager of silicate fibre fabrication. During this time, he received an Australian Research Fellowship from the Australian Research Council (ARC). In 2009, he joined the School of Physics at the University of Sydney as a Queen Elizabeth II Fellow (ARC) where he became the Leader of the Flagship Project "Mid-infrared Photonics" within the ARC Centre of Excellence funded Centre for Ultrahigh-bandwidth Devices for Optical Systems (CUDOS). In early 2014, he moved to the School of Engineering at Macquarie University to take up a permanent position in teaching and optical and photonics engineering research. He is a member of the OSA and AOS and a Senior Member of the IEEE.